# An Autocorrelation Model for Shadow Fading in Rural Macro Environments

Wonsop Kim*, Hyuckjae Lee
Department of Electrical Engineering
Korea Advanced Institute of Science and Technology
Daejeon, Korea
Email: {topsop*, hjlee314}@kaist.ac.kr

Jae Joon Park, Myung-Don Kim, Hyun Kyu Chung
Mobile Telecommunication Research Laboratory
Electronics and Telecommunications Research Institute
Daejeon, Korea
Email: {jjpark, mdkim, hkchung}@etri.re.kr

***Abstract*—We propose an autocorrelation model of SF (shadow fading) in LOS (line-of-sight) rural macro environments. The proposed model is based on the empirical autocorrelations obtained from wideband MIMO (multiple input multiple output) channel measurements at 2.38 and 3.705 GHz. It was found that the SF depends on frequency and so do the empirical autocorrelations. The proposed model provides good matches to empirical autocorrelations in the individual measurement routes.**

***Index Terms*—Correlation, fading channels, measurement, rural areas.**

## I. Introduction

The performance of mobile radio systems is highly dependent on the fading phenomena, FF (fast fading) and SF (shadow fading). The FF results from the superposition of the randomly scattered multipath replicas. The statistical properties of FF have been investigated extensively in the literature [1]. The SF occurs mainly due to the effects of buildings and terrain features and determines the variation of the local mean. Experimental results have shown that SF can be modeled as an RV (random variable) whose logarithm is normally distributed [2], [3].

The autocorrelation behavior of SF is important in mobile communication technologies. For example, the ACF (autocorrelation function) for correlated SF was used to evaluate the performance of a handover algorithm [4], [5], to evaluate the outage probability and spectral efficiency of rate adaptive cellular systems [6], and to design a power control algorithm [7]. Based on the measured data in the urban micro and suburban macro environments, a simple exponential model was proposed in [8] for ACF. Modification of this model for compatibility with the level crossing theory was proposed in [9]. Recently, based on the measured data in the urban macro environments, an autocorrelation model of the SF for the individual measurement routes has been proposed in [2].

This research was supported by the KCC (Korea Communications Commission), Korea, under the R&D program supervised by the KCA (Korea Communications Agency) (KCA-2012-(12-911-01-105)).

This work was supported by the IT R&D program of MKE/KEIT. [10041628, Development of Radio Unit (RU) for multi-band, multi-RAT base stations, based on miniature modular RF units applicable to various cell environments of next generation cellular communications]

TABLE I
BECS 2006 Plus Specification

| Parameter | Frequency [GHz] | Bandwidth [MHz] | PN Length [chips] | Transmitted Power [dBm] |
|---|---|---|---|---|
| Sounder 1 | 2.38 | 20 | 4096 | 37.2 |
| Sounder 2 | 3.705 | 100 | 4096 | 32 |

In this paper, our first contribution investigates the characteristics of the SF from the measured data in the LOS (line-of-sight) rural macro environments at 2.38 and 3.705 GHz. We show that the SF behaviors depend on the frequency and so do the empirical ACFs. In our second contribution, an autocorrelation model of the SF is proposed for the LOS rural macro environments. We show that the proposed model provides good matches to the empirical ACFs in the individual measurement routes.

## II. Measurement Campaign

The measurements were performed at the center frequencies of 2.38 and 3.705 GHz with the BECS (band exploration and channel sounding) 2006 Plus system in Cheongwon and Jeju, Republic of Korea. BECS 2006 Plus utilizes the TDM (time division multiplexing) based transmission (or reception) of PN (pseudo noise) sequences. The sounding procedure can refer to that of the BECS 2005 system found in [10]. The BECS 2006 Plus specification used in the measurements is summarized

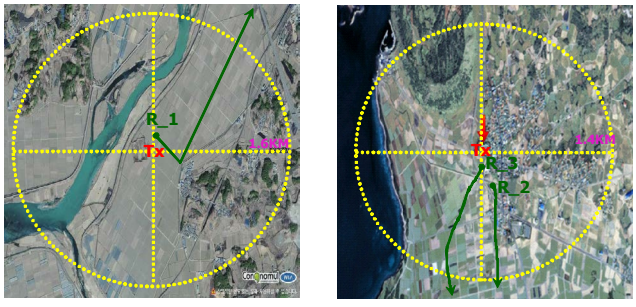


(a) Cheongwon. (b) Jeju.

Fig. 1. Measurement environments. The location of the Tx antenna array is marked with Tx.

TABLE II
MEASUREMENT SCENARIOS

| Scenario | | Antenna spacing [wavelength] | | Antenna height [m] | | Route |
|---|---|---|---|---|---|---|
| | | Tx | Rx | Tx | Rx | |
| 2.38 GHz | C1 | 10 | 0.5 | 25 | 2 | R_1 |
| | J2 | 10 | 0.5 | 27 | 2 | R_2 |
| | J3 | 10 | 0.5 | 27 | 2 | R_3 |
| 3.705 GHz | C4 | 10 | 0.5 | 25 | 2 | R_1 |
| | J5 | 10 | 0.5 | 27 | 2 | R_2 |
| | J6 | 10 | 0.5 | 27 | 2 | R_3 |

in Table I. The Tx (transmit) and Rx (receive) systems use a ULA (uniform linear array) consisting of four antennas, which are four collinear dipoles and four quarter wave monopoles, respectively. Fig. 1 shows the measurement environments, which are characterized as flat terrains consisting of mainly sparsely located houses along roads that lead through fields. As shown in Fig. 1(a), the measurements in Cheongwon were performed along a route (i.e., R_1). As shown in Fig. 1(b), the measurements in Jeju were performed along two routes (i.e., R_2 and R_3). In Fig. 1, the Tx denotes the location of the Tx antenna array. The Rx antenna array was mounted on the roof of a measurement van approximately 2 m above the ground. From the starting point of each route, we drove along each route at a speed of around 10 km/h. Note that we conducted the measurements under very light traffic conditions. Table II shows the measurement scenarios. It is also noted that the measurement at each scenario was conducted separately.

## III. ANALYSIS OF THE MEASUREMENT DATA

In this section, we examine two issues regarding our measurement data. First, we compute the SF from the measured data. Second, we investigate the characteristics of the SF, such as the log-normality and frequency dependence.

### A. Extraction of the Shadow Fading Component

The total received power at a Tx-Rx separation of $d$ in meters is given by

$$P_R(d) = P_D(d) + P_S(d) + P_F(d), \quad (1)$$

where $P_D(d)$ is the component of the received signal strength, which is proportional to the PL (path loss) exponent $n$ and is given by

$$P_D(d) = P_{ref}(d_0) - 10n\log_{10}\left(\frac{d}{d_0}\right), \quad (2)$$

where $P_{ref}(d_0)$ is a reference received power level at the distance $d_0$ from the Tx antennas, $P_S(d)$ is the SF component, $P_F(d)$ is the FF component, and all components are in decibels. The PL in decibels is defined as

$$PL(d) = P_T - P_R(d) + G_T + G_R, \quad (3)$$

where $P_T$, $G_T$, and $G_R$ are the transmitted power, Tx and Rx antenna gains, respectively. In the measurements, The Tx antenna gains for 2.38 and 3.705 GHz are 11 and 12 dBi, respectively. The Rx antenna gains for 2.38 and 3.705 GHz are 0 and 1 dBi, respectively. The single slope log-distance model to estimate the distance dependent PL is expressed as [11]

$$PL_M(d) = 10n\log_{10}(d) + A + B\log_{10}(f_c), \quad (4)$$

where $n$ is the PL exponent, $f_c$ is the center frequency in GHz, $A$ is the interception in decibels, and $B$ describes the frequency dependent factor in decibels. The linear regression using the MMSE (minimum mean square error) criterion was utilized to estimate the $n$, $A$, and $B$ in our measured data, where the fitted parameters are $n = 2.69$, $A = 10.36$, and $B = 33.1$. In order to estimate the SF component, the FF component in $P_R(d)$ needs to be properly removed. Let $P'_R(d)$ denote the averaged received power with the proper window size [12]. It is then assumed that the FF is removed. This means that the received power in decibels approximates the summation of $P_D(d)$ and $P_S(d)$. Thus, the SF component is given by

$$P_S(d) = PL_M(d) - (P_T - P'_R(d) + G_T + G_R). \quad (5)$$

TABLE III
SUMMARY OF STDS OF THE SF

| Window size [wavelength] | | 5 | 10 | 20 | 40 |
|---|---|---|---|---|---|
| STD of SF [dB] | C1 | 2.56 | 2.54 | 2.54 | 2.54 |
| | J2 | 4.10 | 4.10 | 4.09 | 4.08 |
| | J3 | 3.66 | 3.64 | 3.64 | 3.63 |
| | C4 | 1.91 | 1.91 | 1.91 | 1.86 |
| | J5 | 3.38 | 3.37 | 3.37 | 3.37 |
| | J6 | 3.05 | 3.05 | 3.04 | 3.04 |

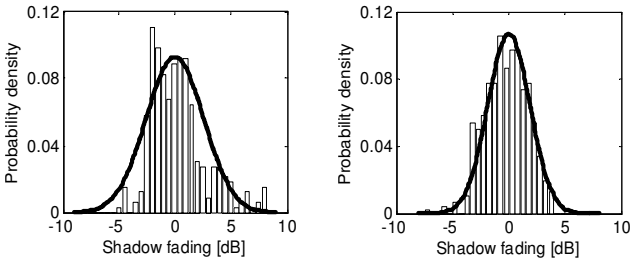


(a) Measured data of C1. (b) Measured data of C4.

Fig. 2. Examples of the SF distribution with a Gaussian fit (solid line).

### B. Characteristics of the Shadow Fading

Let's take the various window sizes for $P_R(d)$ to obtain the appropriate window size. Table III shows the STDs (standard deviations) of the SF component corresponding to the window sizes of 5, 10, 20, and 40$\lambda$, where $\lambda$ is wavelength. The FF component is averaged out if the window size is in a range from 20$\lambda$ to 40$\lambda$. Without loss of generality, we use, throughout this paper, the window size of 40$\lambda$ for averaging out the FF component. The histograms of the SF components in the measured data of C1 and C4 are shown in Fig. 2. The histograms for C1 and C4 are normally distributed with STD $\sigma_{SF}$ = 2.54 dB and $\sigma_{SF}$ = 1.86 dB, respectively.

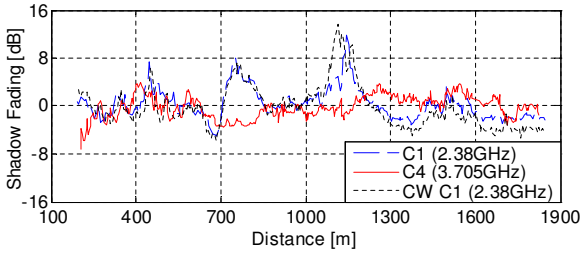


(a) SF components of C1, C4, and CW C1.

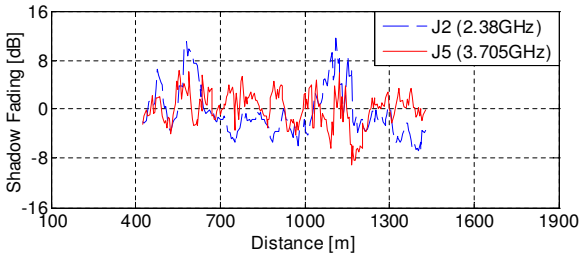


(b) SF components of J2 and J5.

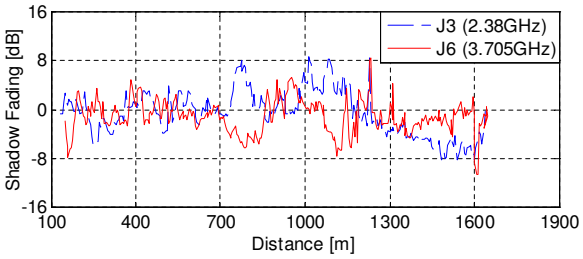


(c) SF components of J3 and J6.

Fig. 3. Variations of the SF components along the routes in Cheongwon and Jeju at 2.38 and 3.705 GHz.

Fig. 3 shows the variations of the SF components along the routes in Cheongwon and Jeju at 2.38 and 3.705 GHz. As a reference, the CW (continuous wave) measurement result performed at Scenario C1 (i.e., the CW C1) is also included in Fig. 3(a). Fig. 3(a) shows that the CW result matches well with the result of C1. It is observed that the SF at 3.705 GHz fluctuates greatly with the low STD, while the SF at 2.38 GHz varies widely with the high STD. Table III also shows that, as the frequency increases, the STDs at each site (i.e., Cheongwon or Jeju) tend to decrease.

Based on these observations (i.e., the fluctuation and STD of the SF), it is expected that the SF is frequency-dependent. A possible explanation is as follows. During the measurements, only the Rx was allowed to move, and, therefore, the SF fluctuation was mainly caused by the changing environment surrounding the Rx. Since the SF fluctuation is a result of the birth and death of multipath, at any given point in space, one path or a set of paths may dominate the received signal. However, as the Rx moves, that signal component becomes attenuated, and another path or set of paths becomes dominant. To explain the frequency dependence of the SF component,

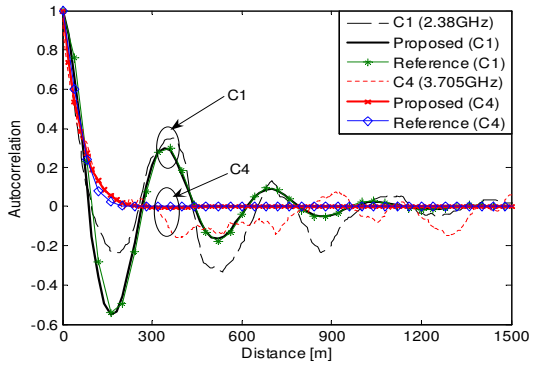


(a) Empirical ACFs of C1 and C4.

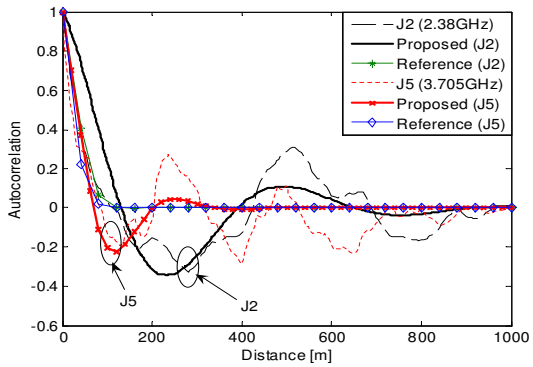


(b) Empirical ACFs of J2 and J5.

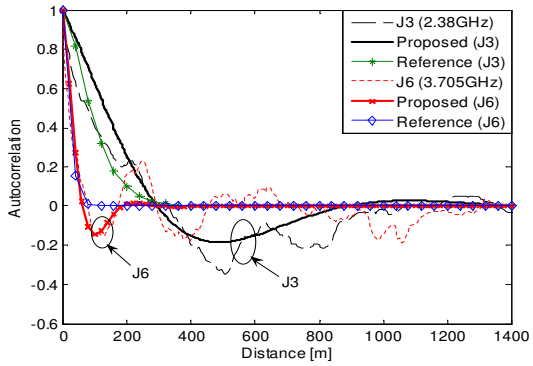


(c) Empirical ACFs of J3 and J6.

Fig. 4. Empirical ACFs of the SF obtained in Cheongwon and Jeju. The proposed EDF model and reference model are fitted to the empirical ACFs. The proposed EDF model provides good matches to the empirical results.

frequency-dependent phenomena such as the diffractions and different reflection coefficients of two frequencies would also be taken into account.

## IV. Autocorrelation Model of Shadow Fading

Let $\mathcal{C} = \{P'_S(1), P'_S(2), ..., P'_S(N)\}$ be the extracted SF samples, where the distance resolution between samples

TABLE IV
FITTED PARAMETERS OF THE PROPOSED MODEL

| Scenarios | | C1 | J2 | J3 | C4 | J5 | J6 |
|---|---|---|---|---|---|---|---|
| Parameters | $d_A$ [m] | 290 | 230 | 317 | 67 | 83 | 58 |
| | $d_B$ [m] | 56 | 83 | 188 | 177 | 43 | 40 |
| | $d_{0.5}$ [m] | 41 | 34 | 76 | 40 | 20 | 19 |

is $\Delta d$ = 40$\lambda$. The ACF of the SF, denoted by $\rho(d_k)$, is then estimated over the set $\mathcal{C}$ at a series of the discrete distance $d_k$ as follows:

$$\rho(d_k) = \left( \frac{\sum_{i=1}^{N-k} P'_S(i) P'_S(i+k)}{\sum_{i=1}^{N} \{P'_S(i)\}^2} \right), \quad (6)$$

where $d_k = k\Delta d$ and $0 \leq k \leq N-1$. Fig. 4 shows the empirical ACFs at each frequency in Cheongwon and Jeju. It is seen that the ACFs at 3.705 GHz rapidly converge to zero, while the ACFs at 2.38 GHz exhibit large fluctuations. This is reasonable since the widely varying SF at 2.38 GHz actually causes the larger fluctuation of the ACF. Based on the visual inspections of the empirical ACFs in the rural macro environments, we propose an EDF (exponentially decreasing fluctuation) function as the autocorrelation model as follows:

$$\rho(d) = \exp\left(-\frac{|d|}{d_A}\right) \cos\left(\frac{|d|}{d_B}\right), \quad (7)$$

where $d_A > 0$ and $d_B > 0$. Fig. 4 also shows the proposed model fitted to the empirical ACFs of the measured data. As a reference, we also include a reference model, which is an autocorrelation model of the SF for the individual measurement routes in the urban macro environments and is represented by [2]

$$\rho(d) = \exp\left(-\frac{|d|}{d_C}\right) \left[\cos\left(\frac{|d|}{d_D}\right) + \frac{d_D}{d_C} \sin\left(\frac{|d|}{d_D}\right)\right], \quad (8)$$

where $d_C > 0$ and $d_D > 0$. The fitted parameters (i.e., $d_A$, $d_B$, $d_C$, and $d_D$) are extracted by using the LSE (least square error) method such that the difference between the measured data and the model is minimized. Clearly, the proposed model matches well with the empirical ACFs of the measured data. Since the ACF is a measure that how fast the local mean power varies as an Rx moves, the proposed model, therefore, provides the correlation information where an Rx moves. Note that since the reference model was proposed based on the measured data in the urban macro environments, the reference model does not fit the empirical ACFs well.

The fitted parameters of the proposed model are summarized in Table IV, where $d_{0.5}$ is the decorrelation distance (i.e., the distance at which the correlation equals 0.5). A short decorrelation distance indicates that the SF changes quickly as the Rx moves, while a longer decorrelation distance corresponds to an environment with a higher degree of stationarity. Table IV shows that the decorrelation distance $d_{0.5}$ at the lower frequency is usually longer than that at the higher frequency. It can also be seen that $d_A$ and $d_B$ of C1, J2, and J3 generally show different characteristics compared to those of C4, J5, and J6. Note that, even though the proposed model for the cases of J2 and J3 does not fit well with $d_{0.5}$ of the measured data, it matches well with the overall fluctuations of the empirical ACFs of J2 and J3 and, therefore, provides significant plus or minus correlation values as the distance increases. Hence, the parameters in (7) can be related to the physical topology of the rural macro environments for the different frequencies.

## V. CONCLUSION

This paper presented the ACFs of the SF in the LOS rural macro environments at 2.38 and 3.705 GHz. It was found that the SF is dependent on the frequency such that the SF at 3.705 GHz fluctuates greatly with the low STD, while the SF at 2.38 GHz varies widely with the high STD. Therefore, the SF at the lower frequency causes a larger fluctuation of the ACF. Based on the measured data, an autocorrelation model was proposed for the LOS rural macro environments. The proposed model matches well with the empirical ACFs of the individual routes.

## REFERENCES


[1] G. L. Stüber, *Principles of Mobile Communication*, Boston, MA: Kluwer Academic, 1996.

[2] Y. Zhang, J. Zhang, D. Dong, X. Nie, G. Liu, and P. Zhang, "A novel spatial autocorrelation model of shadow fading in urban macro environments," in *Proc. of IEEE Global Telecommunications Conference (GLOBECOM)*, pp. 1–5, Nov. 2008.

[3] IST-4-027756 WINNER II D1.1.1, "WINNER II interim channel models," v1.1, Nov. 2006.

[4] K.-I. Itoh, S. Watanabe, J.-S. Shih, and T. Sato, "Performance of handoff algorithm based on distance and RSSI measurements," *IEEE Trans. Veh. Technol.*, vol. 51, no. 6, pp. 1460–1468, Nov. 2002.

[5] H.-P. Lin, R.-T. Juang, and D.-B. Lin, "Validation of an improved location-based handover algorithm using GSM measurement data," *IEEE Trans. Mobile Comput.*, vol. 4, no. 5, pp. 530–536, Sep.-Oct. 2005.

[6] K. Yamamoto, A. Kusuda, and S. Yoshida, "Impact of shadowing correlation on coverage of multihop cellular systems," in *Proc. of IEEE International Conference on Communications (ICC)*, pp. 4538–4542, Jun. 2006.

[7] K. Shoarinejad, J. L. Speyer, and G. J. Pottie, "Integrated predictive power control and dynamic channel assignment in mobile radio systems," *IEEE Trans. Wireless Commun.*, vol. 2, no. 5, pp. 976–988, Sep. 2003.

[8] M. Gudmundson, "Correlation model for shadow fading in mobile radio systems," *Electron. Lett.*, vol. 27, no. 23, pp. 2145–2146, Nov. 1991.

[9] D. Giancritofaro, "Correlation model for shadow fading in mobile radio channels," *Electron. Lett.*, vol. 32, no. 11, pp. 958–959, May 1996.

[10] J. J. Park, W. S. Kim, M. D. Kim, and H. K. Chung, "Measurement results at 3.7 GHz in urban macrocell environment," in *Proc. of IEEE Vehicular Technology Conference (VTC)*, pp. 864–868, Sep. 2007.

[11] IST-4-027756 WINNER II D1.1.2, "WINNER II channel models: Part I channel models," v1.2, Sep. 2007.

[12] X. Zhao, J. Kivinen, P. Vainikainen, and K. Skog, "Propagation characteristics for wideband outdoor mobile communications at 5.3 GHz," *IEEE J. Sel. Areas Commun.*, vol. 20, no. 3, pp. 507–514, Apr. 2002.